Loading rates and the dynamic initiation toughness in brittle solids

C. LIU[1], W.G. KNAUSS[2] and A.J. ROSAKIS[2]
[1]*Materials Science and Technology Division, MS-G755, Los Alamos National Laboratory, Los Alamos, New Mexico 87545, U.S.A.*
[2]*Graduate Aeronautical Laboratories, 105-50, California Institute of Technology, Pasadena, California 91125, U.S.A.*

Abstract. The experimentally determined marked rise of the stress intensity factor required to initiate crack propagation in brittle solids under variably high loading rates, is analyzed. This problem of fracture initiation at the tip of a crack is considered in terms of activating a flaw at some distance away from the tip. By using a semi-infinite crack in an unbounded two-dimensional solid subjected to spatially uniform but temporally varying crack-face pressure, we consider the evolution of stress at the failure initiation site. Fracture initiation is assumed synonymous with attaining a critical stress at the fracture site. The results conform to typical experimental data of dynamic crack initiation in brittle solids.

Key words: Dynamic fracture, initiation toughness, brittle fracture.

1. Introduction

When crack tips in brittle materials are subjected to increasingly higher loading rates or shorter stress pulses, the stress level needed for initial crack propagation increases sharply (Smith, 1975; Ravi-Chandar and Knauss, 1984). A similar phenomenon has been observed by Shockey and his colleagues (Kalthoff and Shockey, 1977; Homma et al., 1983; Shockey et al., 1983; 1986) in the initiation and spread of damage under conditions leading to spall. Although they have explained their experimental results through material rate dependence, such an observation is initially surprising in that one does not expect such a strongly time dependent response in a material that exhibits no apparent intrinsic rate sensitive behavior. In defence of this rate dependent material modeling, it must be recognized that the crack initiation phenomenon occurs typically on a spatially very small size scale within which material properties are not often measured directly and are thus not necessarily well established, especially not under high deformation rates. On the other hand it is appropriate to examine whether such time dependent effects can arise from wave phenomena alone while retaining (linearly) elastic constitutive behavior and brittle fracture response in the analysis. In fact, we shall see that such consideration can well explain the apparent rate dependence of the fracture initiation process.

Steverding and Lehnigk (1970) have suggested without further physical explanations that this phenomenon is governed by a 'critical impulse criterion' such that the product of the crack-tip stress to a certain power and the pulse duration be a constant. Alternately, Petrov and Morozov (1994) have postulated a 'structure-time criterion' that requires a (micro) structure based time, τ, which is not identified further and needs to be determined individually for each
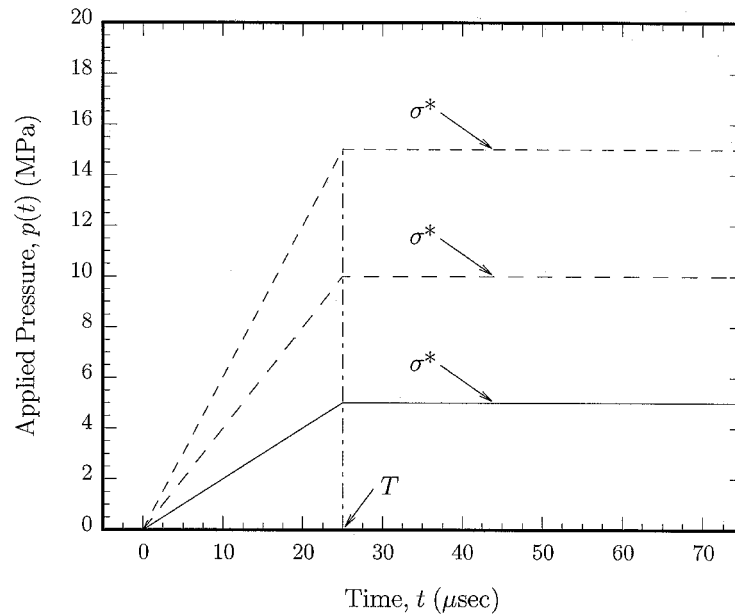
Figure 1. Time history of applied pressure used in the experimental study.

material, as well as a structural size parameter estimated from $d = 2K_{\text{IC}}^2/\pi\sigma_c^2$, where K_{IC} is the quasistatic fracture toughness. In analyzing the data from Ravi-Chandar and Knauss (1984) they assumed implicitly, however, that the near-tip field is governed by the stress intensity factor, which assumption is not valid inasmuch as the stress field there possesses highly transient characteristics (Ma and Freund, 1986; Ravi-Chandar and Knauss, 1987).

Here we examine the effect of the interaction of this temporally evolving stress field at the tip of a macroscopic crack with small defects in its vicinity, where are allowed to grow once a stress has been achieved that is critical for their size or severity. Such cracks are then understood to grow and coalesce rapidly thereby effecting the growth of the macroscopic crack.

Following Smith (1975), Ravi-Chandar and Knauss (1984) conducted experiments on large plates of Homalite-100 (a brittle Polyester) simulating the infinite domain for the duration of the experiment, which arrangement allowed the use of Freund's exact analysis derived for the infinite elastic plane (Freund, 1972). Loading was achieved in the experiments through an electro-magnetic device (Lorentz force generator) for imparting spatially uniform pressure histories to the crack faces that can be well approximated by ramps possessing constant rise times of 25 μsec. Through varying the magnitude of the final pressure the rate of loading could be varied as illustrated in Figure 1. By recording the caustic patterns at the crack tip through high speed photography the history of the stress intensity was recorded (see Ravi-Chandar and Knauss, 1982). Results from Ravi-Chandar and Knauss (1984) are rendered in Figure 2 showing the stress intensity factor at the time the crack began to propagate which illustrates clearly the sharp rise in the stress intensity factor as the crack propagation initiation moves to shorter times.

It will be the purpose of the following exposition to 'explain' the phenomenon of rate dependence of the dynamic initiation toughness of brittle solids, in mechanics terms of transient
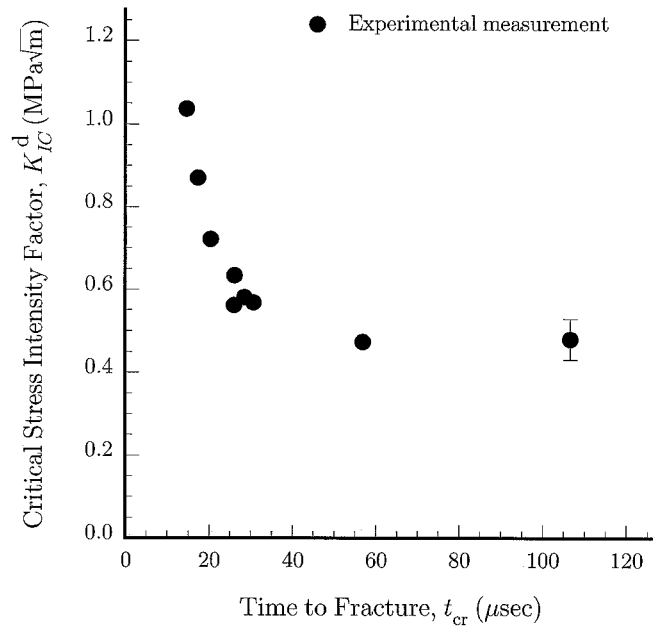
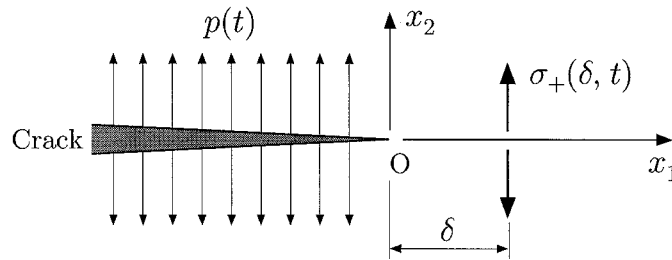*Figure 2.* Variation of the stress intensity factor required for initiation against the time to fracture.

Figure 3. A semi-infinite crack subjected to uniformly distributed pressure on its surface that varying with time t.

wave motion in the elastic domain around the tip of the initially stationary crack, and without invoking any intrinsic time dependence of the material.

2. The model

To demonstrate the feasibility of the concept proposed in the introduction, we consider, with reference to Figure 3, the following situation: A semi-infinite crack is located in an infinite medium with its tip at $x_1 = 0$ and $x_2 = 0$. A defect is located at a small distance δ ahead of this tip. The crack flanks are subjected to a spatially uniform pressure $p(t)$ of timewise varying magnitude. The defect breaks into a growing (micro) crack when the stress level, in particular the stress $\sigma_+(\delta, t)$ at the point $(x_1 = \delta, x_2 = 0)$, reaches a value σ_{cr}, which happens at some time t_{cr} to be determined. It is of interest then to determine the transient tensile traction at the point $x_1 = \delta$. To this end it will be insufficient to consider only the time-varying stress intensity field, because for very short times that field will not have spread sufficiently far to engulf the defect (see discussions of K_I-dominance in Ravi-Chandar and Knauss, 1987 and

Krishnaswamy and Rosakis, 1991). We are thus, specifically, interested in determining the stress rise history at $x_1 = \delta$.

A word is in order with respect to the chosen pressure distribution over the (semi-infinite) crack flanks. Because of the infinite extent of the boundary loading we expect that for infinite time the moment acting on the infinite solid is unbounded, so that the solution offered below does not have a long-time static limit. However, this fact has no essential consequence for this demostration, since we are only interested in relatively short times after the loading is applied. The present approach should render a reasonable evaluation of whether the proposed physics has relevance to dynamic fracture initiation in ideally brittle, rate insensitive material.

In more realistic situations it may be necessary to consider not only a single flaw in the crack-tip region. Instead, it is probably more correct to allow for statistical distributions of defects with respect to both severity and space. We believe, however, that the current simpler model illustrates the behavior attached to the stress-wave-and-flaw-interaction concept.

3. Transient stress field around the crack tip

Let $\mathcal{R}$ be an unbounded two dimensional region occupied by a body composed of an isotropic, homogeneous, linearly elastic material. The body contains a straight semi-infinite crack located in $-\infty < x_1 \leqslant 0, x_2 = 0$, see Figure 3. For time $t < 0$, the body is stress free and at rest everywhere. At time $t = 0$, a uniformly distributed pressure with magnitude $p(t)$, is applied on the crack flanks. For planar deformation, two displacement potentials, $\phi(x_1, x_2, t)$ and $\psi(x_1, x_2, t)$, exist such that the two in-plane non-zero displacement components can be expressed through

$$u_\alpha(x_1, x_2, t) = \phi_{,\alpha}(x_1, x_2, t) + e_{\alpha\beta}\psi_{,\beta}(x_1, x_2, t), \quad \forall(x_1, x_2) \in \mathring{\mathcal{R}}, \quad t > 0, \tag{3.1}$$

where $\mathring{\mathcal{R}} = \mathcal{R} - \{-\infty < x_1 \leqslant 0, x_2 = 0\}$, and $\alpha, \beta \in \{1, 2\}$. The summation convention is used here and $e_{\alpha\beta}$ is the two dimensional alternator. The nominal stress components are given by

$$
\left.
\begin{aligned}
\sigma_{11} &= \mu \left\{ \frac{c_l^2}{c_s^2}\phi_{,\alpha\alpha} - 2\phi_{,22} + 2\psi_{,12} \right\} \\
\sigma_{22} &= \mu \left\{ \frac{c_l^2}{c_s^2}\phi_{,\alpha\alpha} - 2\phi_{,11} - 2\psi_{,12} \right\} \\
\sigma_{12} &= \mu \{ 2\phi_{,12} + \psi_{,22} - \psi_{,11} \}
\end{aligned}
\right\}, \quad \forall(x_1, x_2) \in \mathring{\mathcal{R}}, \quad t > 0, \tag{3.2}
$$

where μ is the shear modulus, and c_l and c_s are the dilatational and shear wave speeds of the elastic material, respectively, given by

$$c_l = \left\{ \frac{\kappa + 1}{\kappa - 1} \cdot \frac{\mu}{\rho} \right\}^{1/2}, \quad c_s = \left\{ \frac{\mu}{\rho} \right\}^{1/2}, \tag{3.3}$$

where $\kappa = 3 - 4\nu$ for plane strain and $\kappa = (3 - \nu)/(1 + \nu)$ for plane stress, with ρ being the mass density and ν the Poisson's ratio of the elastic solid.

In terms of the two displacement potentials, $\phi(x_1, x_2, t)$ and $\psi(x_1, x_2, t)$, the equations of motion in the absence of body force density are

$$\left. \begin{array}{l} \phi_{,\alpha\alpha}(x_1, x_2, t) - a^2 \ddot{\phi}(x_1, x_2, t) = 0 \\[2mm] \psi_{,\alpha\alpha}(x_1, x_2, t) - b^2 \ddot{\psi}(x_1, x_2, t) = 0 \end{array} \right\}, \quad \forall (x_1, x_2) \in \overset{\circ}{\mathcal{R}}, \quad t > 0, \tag{3.4}$$

where $a = 1/c_l$ and $b = 1/c_s$. The boundary conditions are

$$\left. \begin{array}{ll} \sigma_{22}(x_1, 0^{\pm}, t) = -p(t), & -\infty < x_1 \leqslant 0 \\[2mm] \sigma_{12}(x_1, 0^{\pm}, t) = 0, & -\infty < x_1 < \infty \\[2mm] u_2(x_1, 0^{\pm}, t) = 0, & 0 < x_1 < \infty \end{array} \right\}, \quad t > 0, \tag{3.5}$$

while the initial conditions are

$$\left. \begin{array}{l} \phi(x_1, x_2, 0) = \psi(x_1, x_2, 0) = 0 \\[2mm] \dot{\phi}(x_1, x_2, 0) = \dot{\psi}(x_1, x_2, 0) = 0 \end{array} \right\}, \quad \forall (x_1, x_2) \in \overset{\circ}{\mathcal{R}} . \tag{3.6}$$

The requirement that the displacements should be bounded throughout the region, or that the mechanical energy density be integrable allows, nevertheless, that the stresses at the crack tip be singular, so that we have

$$\int_{\mathcal{R}'} (\sigma_{\alpha\beta}\varepsilon_{\alpha\beta} + \rho \dot{u}_\alpha \dot{u}_\alpha) \, \mathrm{d}A < \infty, \quad \forall \mathcal{R}' \subset \overset{\circ}{\mathcal{R}} . \tag{3.7}$$

In agreement with Figure 4, the pressure applied to the crack faces, $p(t)$, is assumed to have the (ramp) form

$$p(t) = \begin{cases} \frac{\sigma^* t}{T}, & 0 < t < T, \\[2mm] \sigma^*, & t \geqslant T, \end{cases} \tag{3.8}$$

where T represents the finite rise time. To obtain the solution for the normal traction ahead of the crack tip, we obtain first the solution corresponding to $T = 0$ (step function profile) from which the final solution can be easily constructed.

3.1. SOLUTION FOR THE STEP PRESSURE

For the pressure

$$p(t) = \sigma^* H(t), \tag{3.9}$$

with $H(\cdot)$ denoting the Heaviside step function, the normal traction ahead of the stationary crack tip, $\sigma_+(x_1, t)$, can be obtained as (Freund, 1990),

$$\sigma_+(x_1, t) = -\frac{\sigma^*}{\pi} \cdot \frac{\sqrt{2(1 - 2\nu)}}{2(1 - \nu)}$$

$$\int_{ax_1}^{t} \frac{\frac{c}{a} - \frac{\eta}{ax_1}}{\sqrt{\frac{\eta}{ax_1} - 1}} \cdot \frac{S_+\left(-\frac{\eta}{x_1}\right)}{\eta} \, \mathrm{d}\eta \cdot H(t - ax_1), \tag{3.10}$$
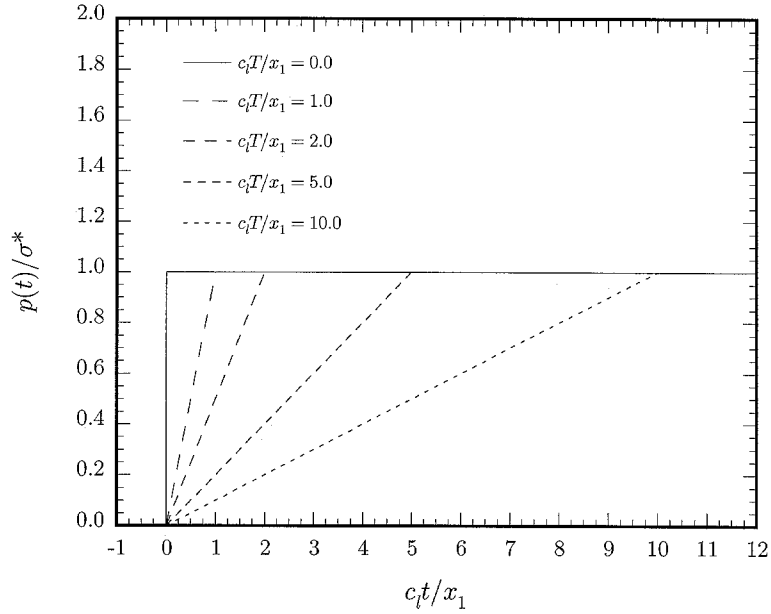
Figure 4. Profiles of the pressure applied on the surface of a semi-infinite stationary crack. T represents the finite rise time of the loading.

where $c = 1/c_R$ and c_R is the Rayleigh wave speed of the elastic solid determined from

$$D(v) \equiv 4\left(1 - \frac{v^2}{c_l^2}\right)^{1/2}\left(1 - \frac{v^2}{c_s^2}\right)^{1/2} - \left(2 - \frac{v^2}{c_s^2}\right)^2 = 0. \tag{3.11}$$

In expression (3.10), the function $S_+(\zeta)$ is defined by

$$S_+(\zeta) = \exp\left\{-\frac{1}{\pi}\int_a^b \tan^{-1}\left[\frac{4x^2\sqrt{(x^2 - a^2)(b^2 - x^2)}}{(b^2 - 2x^2)^2}\right]\frac{\mathrm{d}x}{x + \zeta}\right\}. \tag{3.12}$$

The distribution of the normal traction $\sigma_+(x_1, t)$ under the surface pressure (3.9) is plotted in Figure 5, for $v = 0.3$, assuming plane stress conditions. In addition, the arrival of each wave is indicated in the figure as well. The stress intensity factor at the crack tip, $K_I(t)$ corresponding to the step pressure situation is

$$K_I(t) = \frac{2\sigma^*}{1 - v}\sqrt{\frac{(1 - 2v)c_l t}{\pi}}. \tag{3.13}$$

3.2. CRACK FACE PRESSURE WITH FINITE RISE TIME

Based on the solution for the step crack-face pressure, solutions for ramp loadings (3.8), can be obtained by superposition. The normal traction ahead of the stationary crack tip is then

$$\frac{\sigma_+(x_1, t)}{\sigma^*} = \begin{cases} \int_0^{t/T} G\left(\frac{T}{ax_1}\left(\frac{t}{T} - \eta\right)\right)\mathrm{d}\eta, & 0 < t < T, \\[4mm] \int_0^1 G\left(\frac{T}{ax_1}\left(\frac{t}{T} - \eta\right)\right)\mathrm{d}\eta, & t \geqslant T, \end{cases} \tag{3.14}$$
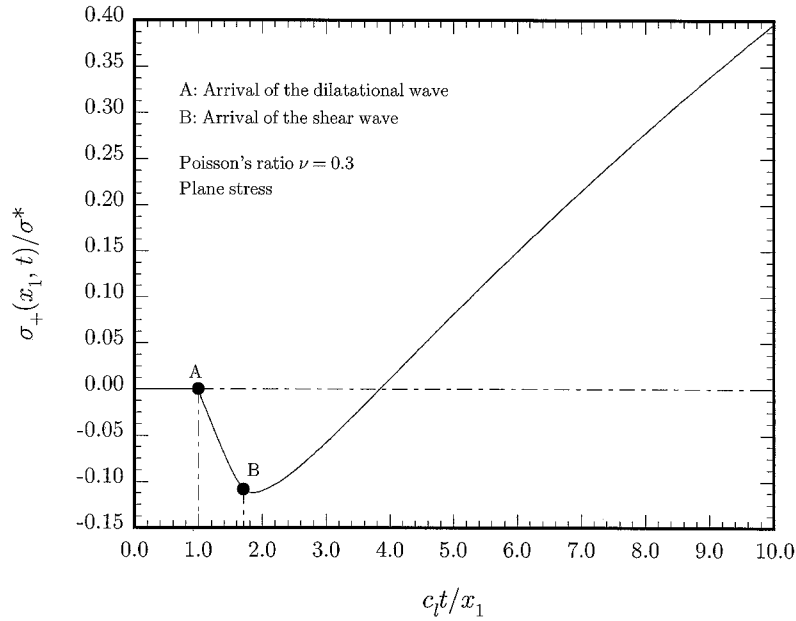
Figure 5. Variation of the normal traction ahead of the stationary crack tip for plane stress. The crack-face pressure has the step function profile.

where

$$G(\xi) = \int_0^{\sqrt{\xi-1}} \tau_b(\lambda) \, d\lambda \cdot H(\xi - 1),$$

and

$$\tau_b(\lambda) = -\frac{\sqrt{2(1 - 2\nu)}}{\pi(1 - \nu)} \left\{ \left(\frac{c}{a} - 1\right) - \lambda^2 \right\} \frac{S_+(-a(1 + \lambda^2))}{1 + \lambda^2}.$$

Now, the stress intensity factor at the crack tip is given by

$$\frac{K_I(t)}{\sigma^*\sqrt{\pi c_l T}} = \begin{cases} \dfrac{4\sqrt{1 - 2\nu}}{3\pi(1 - \nu)} \left(\dfrac{t}{T}\right)^{3/2}, & 0 < t < T, \\[4mm] \dfrac{4\sqrt{1 - 2\nu}}{3\pi(1 - \nu)} \left\{ \left(\dfrac{t}{T}\right)^{3/2} - \left(\dfrac{t}{T} - 1\right)^{3/2} \right\}, & t \geqslant T. \end{cases} \tag{3.15}$$

The normal traction ahead of the crack tip is plotted in Figure 6 for ramp pressure loading. As in Figure 5, only plane stress solutions are shown for $\nu = 0.3$. For comparison purposes, the distribution for $T = 0$ is presented as well. Note that for various values of T, the initial normal traction is all negative and decreasing, it increases at the moment when the shear wave arrives. The initial increase is rather slow until the loading signal corresponding to the plateau portion of the pressure function arrives. Also notice that the final increasing rate of the normal traction is almost the same for all the values of T. In Figure 7, the stress intensity factor at the stationary crack tip is plotted as a function of time t. From this figure one can see that when
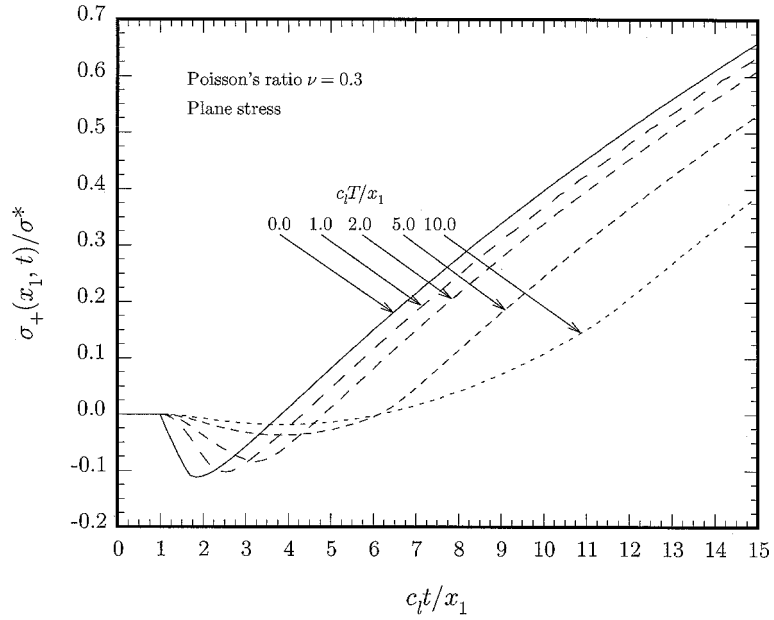
Figure 6. Distribution of the normal traction ahead of the tip of a semi-infinite stationary crack that is subjected to uniform pressure with finite rise time (plane stress).
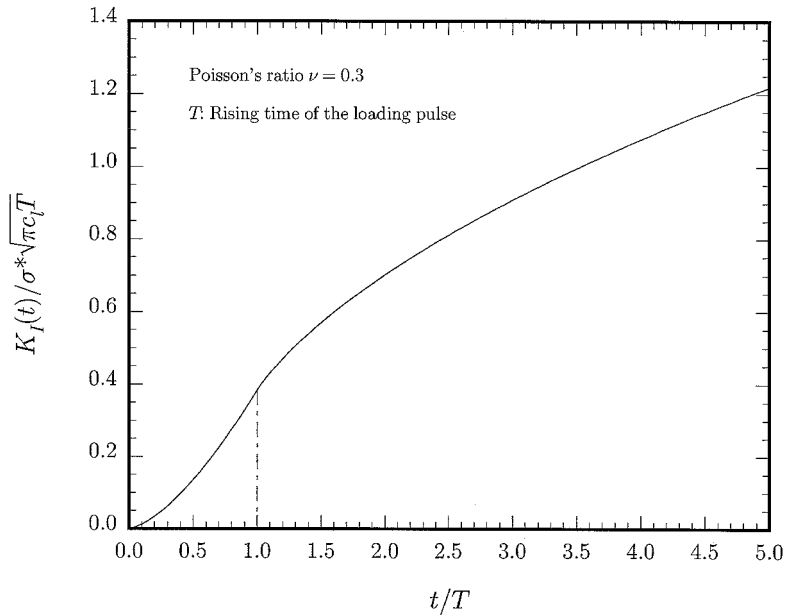

Figure 7. Variation of the stress intensity factor at the stationary crack tip, K_{I}, as a function of time t.
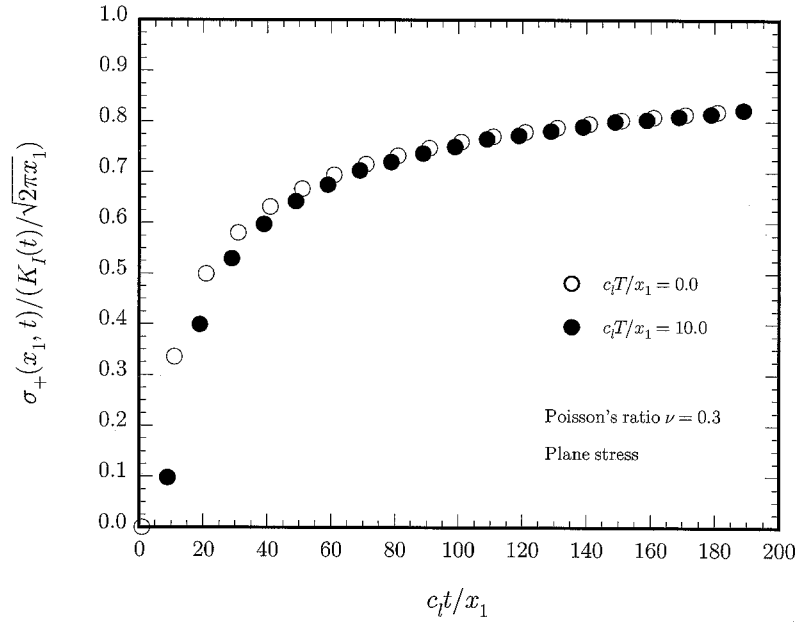
Figure 8. Comparison of the transient traction solution with its K_I-dominant representation.

$t/T < 1$, the quantity $\dot{K}_I(t)$, which provides the measure of loading rate at the crack tip, is an increasing function of time t, while for $t/T > 1$, $\dot{K}_I(t)$ decreases with respect to time t.

To study the region of K_I-dominance, the ratio of the normal traction ahead of the crack tip, $\sigma_+(x_1, t)$, to the quantity $K_I(t)/\sqrt{2\pi x_1}$, which is the leading term in the asymptotic representation of the stress field, is plotted against $c_l t/x_1$ in Figure 8. Only two values of the rise time T are considered, one for the step loading case ($T = 0$, open circles), and one for nonzero T (solid circles). One observes that for the normal traction to approach its K_I-dominant representation at a fixed point ahead of the crack tip, an extremely long time is needed. On the other hand, for fixed time t, the K_I-dominant solution is applicable only at points that are very close to the crack tip. Therefore, at a finite distance from the crack tip and at moments of earlier stages of loading, no region exists that can be described accurately by the leading term of the asymptotic solution alone. This observation is at the heart of the apparent rate dependence of the initiation time.

4. Dynamic crack initiation

As discussed in the introduction, we view the inititation of a stationary crack as a process that the defects in the vicinity of the crack tip develop into small secondary cracks, and these secondary cracks coalesce with the original crack so as to enlarge it further. The formation of the secondary cracks in the vicinity of the crack tip is controlled by the stress level at that location. It is also believed that this process is closely connected to how the stress level reaches the critical value, *i.e.*, the loading history at the location of the defects. In this section, the effect of loading rate on the dynamic initiation toughness of a stationary crack is considered using the model problem solved in the previous section.

In the previous section, we determined the transient stress field surrounding the tip of a semi-infinite crack in an unbounded region. The surface of the crack is subjected to a spatially
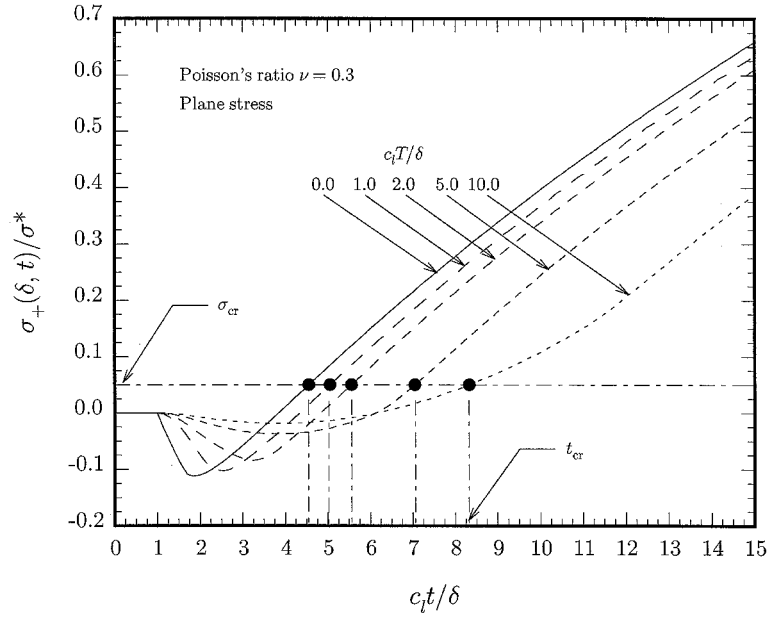
Figure 9. Variation of the normal traction at the location $x_1 = \delta$ ahead of the stationary crack tip for different rise times T. At time t_{cr}, the critical stress σ_{cr}, under which the defect breaks into secondary crack, is reached.

uniform but timewise varying pressure. The crack face pressure $p(t)$ is characterized by its peak value σ^* and the rise time T. The normal traction ahead of the stationary crack tip is given in (3.14), and its variation is shown in Figure 6. Now consider a defect located at a small distance δ ahead of the stationary crack tip. The variation of the normal stress at the location $x_1 = \delta$ is plotted in Figure 9 against the time t for different rise times T. Suppose that at the stress level σ_{cr}, the defect breaks into a secondary crack, i.e., the critical condition for formation of secondary cracks is

$$\sigma_+(\delta, t_{\mathrm{cr}}) = \sigma_{\mathrm{cr}}. \tag{4.1}$$

For a given rise time T and the critical stress σ_{cr}, from

$$\frac{\sigma_{\mathrm{cr}}}{\sigma^*} = \begin{cases} \displaystyle\int_0^{t_{\mathrm{cr}}/T} G\left(\frac{T}{a\delta}\left(\frac{t_{\mathrm{cr}}}{T} - \eta\right)\right) \mathrm{d}\eta, & 0 < t_{\mathrm{cr}} < T, \\[4mm] \displaystyle\int_0^1 G\left(\frac{T}{a\delta}\left(\frac{t_{\mathrm{cr}}}{T} - \eta\right)\right) \mathrm{d}\eta, & t_{\mathrm{cr}} \geqslant T, \end{cases} \tag{4.2}$$

where the function $G(\cdot)$ has been defined in the previous section, the critical time t_{cr} can be determined as a function of the rise time T for different ratios of $\sigma_{\mathrm{cr}}/\sigma^*$ and is plotted in Figure 10. For a given rise time T and the critical stress σ_{cr}, together with the critical time t_{cr} established from (4.2) and Figure 10, the apparent dynamic fracture toughness, $K_{\mathrm{IC}}^{\mathrm{d}}$, is calculated from

$$\frac{K_{\mathrm{IC}}^{\mathrm{d}}}{\sigma^*\sqrt{\pi c_l T}} = \begin{cases} \dfrac{4\sqrt{1 - 2\nu}}{3\pi(1 - \nu)}\left(\dfrac{t_{\mathrm{cr}}}{T}\right)^{3/2}, & 0 < t_{\mathrm{cr}} < T, \\[4mm] \dfrac{4\sqrt{1 - 2\nu}}{3\pi(1 - \nu)}\left\{\left(\dfrac{t_{\mathrm{cr}}}{T}\right)^{3/2} - \left(\dfrac{t_{\mathrm{cr}}}{T} - 1\right)^{3/2}\right\}, & t_{\mathrm{cr}} \geqslant T. \end{cases} \tag{4.3}$$
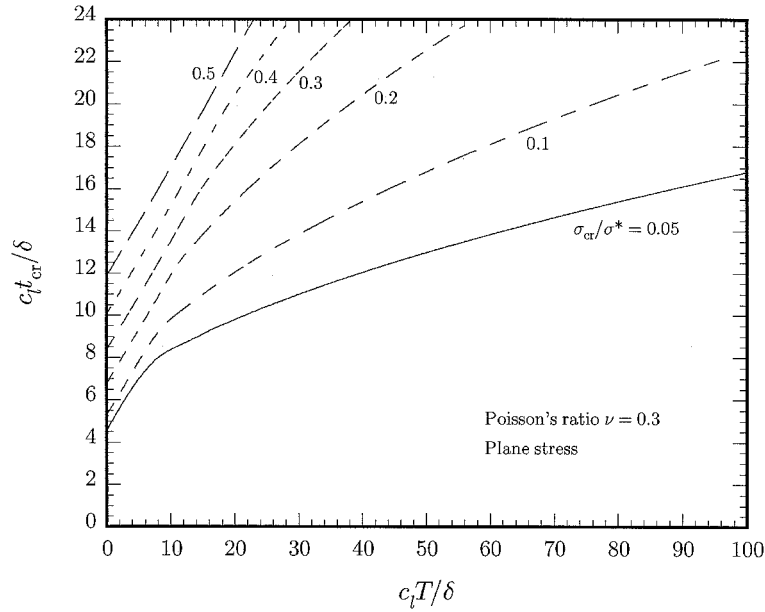
Figure 10. Variation of the critical time t_{cr}, at which the secondary cracks are formed, as a function of the rise time T for different ratios of σ_{cr}/σ^*.

This apparent stress intensity factor at the moment of crack initiation, for a fixed ratio σ_{cr}/σ^*, is plotted as solid circles in Figure 11 for different rise times. Note that for the given critical stress level σ_{cr}, the apparent initiation toughness is almost a constant for small values of critical time t_{cr}, and then drops drastically when the critical time t_{cr} becomes larger. The transition occurs when the critical time $t_{cr} = T$. The prefracture variation of the stress intensity factor at the stationary crack tip, as a function of time, is also shown in Figure 11 ending at the solid circles: for each $c_l T/\delta$ and given σ^*, the stress intensity factor K_I is an increasing function of time t until $t = t_{cr}$ when the crack starts to propagate.

Several observations are appropriate. Figure 12 describes the relation between the apparent fracture toughness K_{IC}^d and the critical time t_{cr} at which the crack initiates for different critical stresses σ_{cr}. The apparent fracture toughness K_{IC}^d is normalized by the quantity $K_{IC}^s = \sigma_{cr}\sqrt{2\pi\delta}$ in Figure 12. Note that all the curves collapse into a single one when $t_{cr} > T$ for different critical stresses σ_{cr}. Meanwhile, after the moment when the critical time t_{cr} is comparable to the rise time T, the fracture toughness K_{IC}^d decreases with the increase in the critical time t_{cr}. Another way to examine the effect of the critical stress σ_{cr} on the apparent fracture toughness is presented in Figure 13. With respect to a fixed position ahead of the stationary crack tip, for any given rise time T of the loading pressure and any critical time t_{cr}, the apparent fracture toughness K_{IC}^d is completely determined from (4.3). This relation can be described by a surface $K_{IC}^d = K_I(t_{cr}, T)$, as shown in Figure 13. However, for a given critical stress σ_{cr}, as determined in independent experimental measurements say, or from micromechanical analysis, the critical time t_{cr} should be determined through (4.2) for the fixed position ahead of the stationary crack tip, δ. Now the relation between the apparent fracture toughness K_{IC}^d, critical time t_{cr}, and rise time T will be a curve on the surface in Figure 13, which is represented by the solid circles in the figure. From the above observations, one appreciates that as the critical time t_{cr} becomes larger than the rise time of the applied
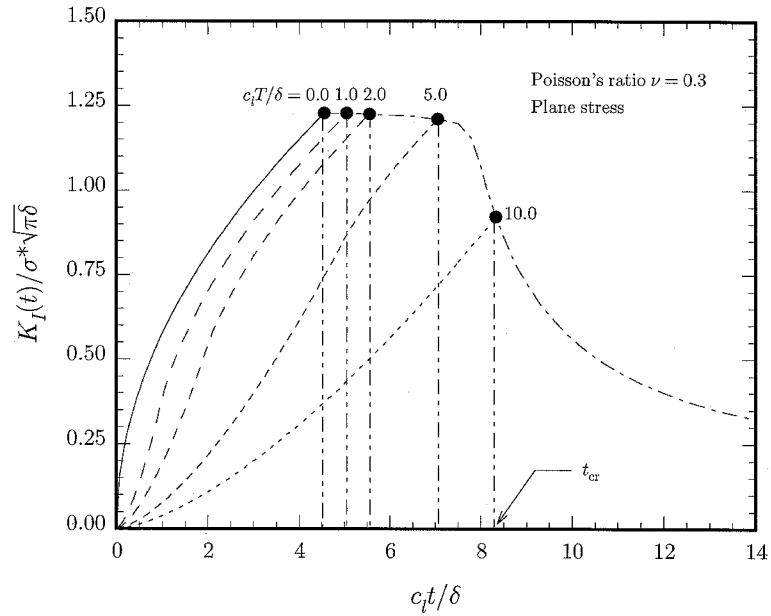
Figure 11. Variation of the stress intensity factor $K_I(t)$ at the stationary crack tip. For the given critical values of σ_{cr} and T_{cr}, the apparent fracture toughness K_I^d can be obtained for different rise times T.
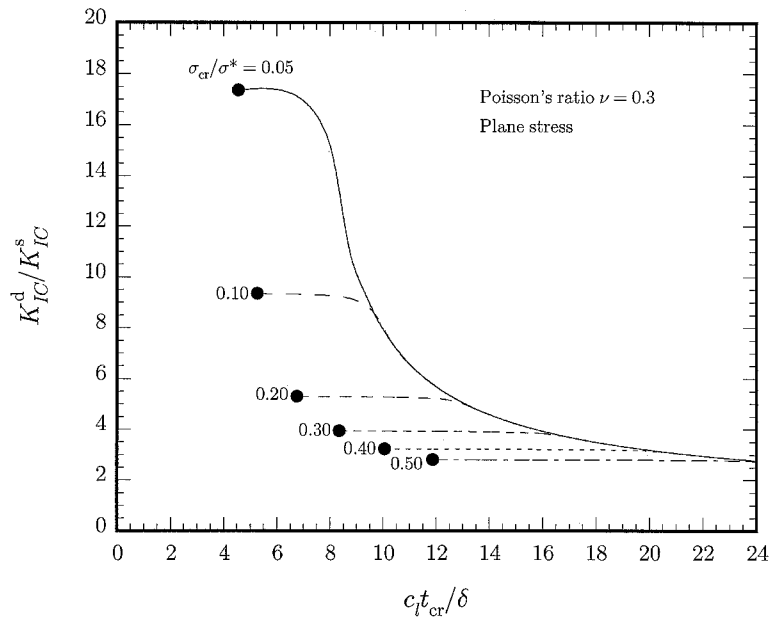

Figure 12. Variation of the apparent fracture toughness K_{IC}^d, as a function of the critical time t_{cr} for different critical stresses σ_{cr}.
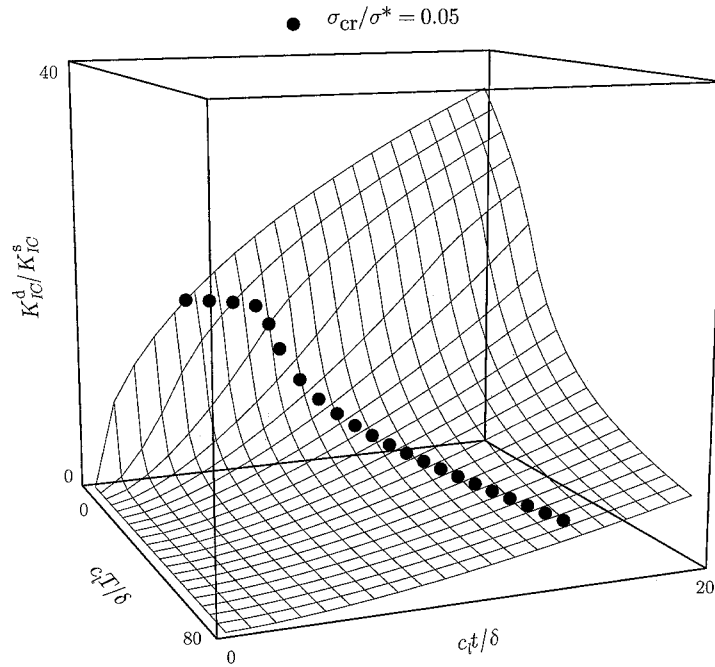
Figure 13. Complete relation between the apparent fracture toughness K_{IC}^{d}, rise time T, critical time t_{cr}, and the critical stress σ_{cr}.
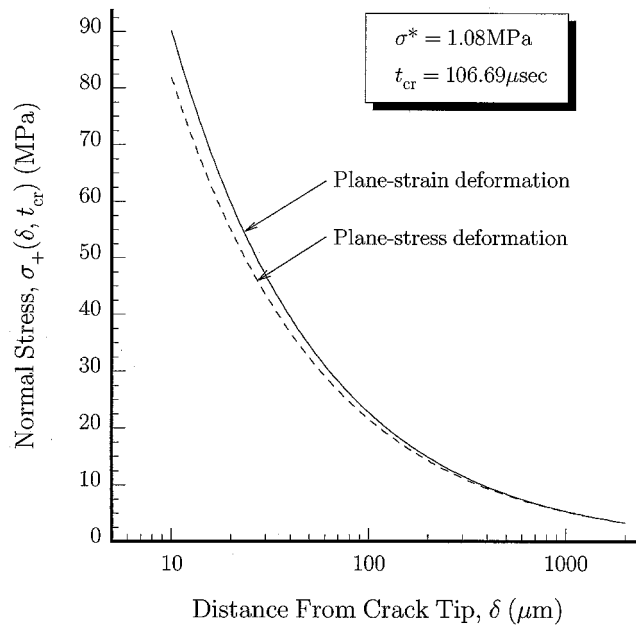

Figure 14. Variation of the normal stress ahead of the stationary crack tip at the moment of crack inititiation, as a function of the distance from the crack tip.
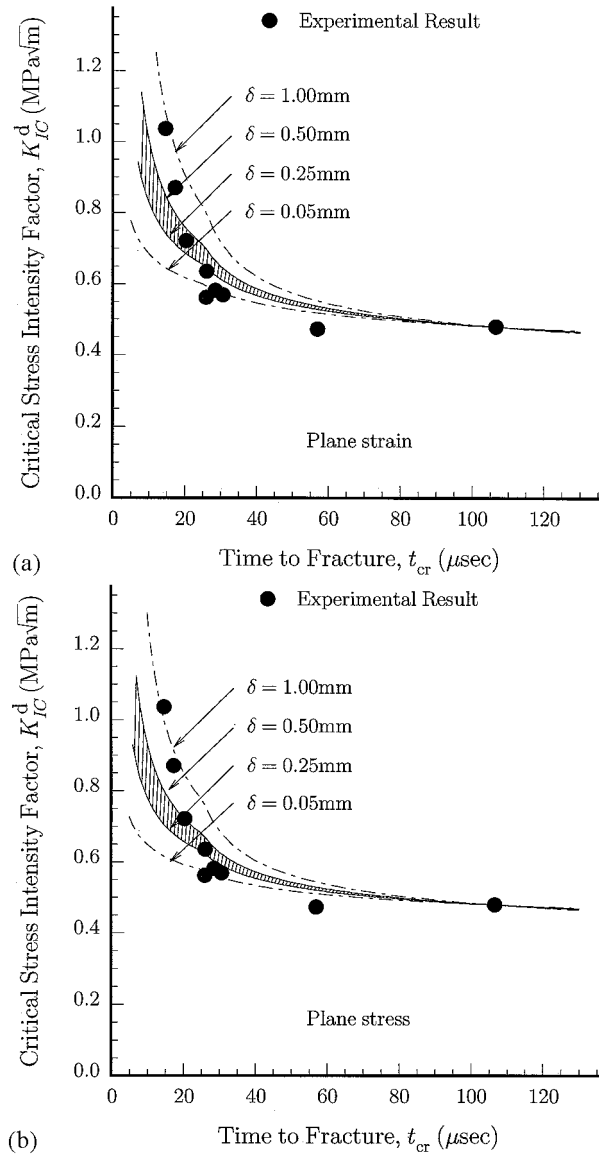
Figure 15. Relationship between K_{IC}^d and t_{cr} from analytical calculations and from experimental measurements: (a) plane-strain, (b) plane-stress.

stress T, the apparent fracture toughness K_{IC}^d is a decreasing function. If we identify t_{cr} as the moment at which the crack starts to propagate, these observations are in agreement with the experimental measurements on Homalite-100 material by Ravi-Chandar and Knauss (1984).

5. Comparison with experiments

To compare the experimental observations of Ravi-Chandar and Knauss (1984) to the theoretical analysis discussed in the previous section, we need to know first the traction distribution along the line ahead of the stationary crack tip at the moment of crack initiation. For the case

$\sigma^* = 1.08$ MPa and $t_{\text{cr}} = 106.69\,\mu\text{sec}$, according to (3.14), the distribution of the normal stress at the moment of crack initiation t_{cr}, is plotted in Figure 14 for material parameters of Homalite-100 ($c_l = 2057$ m/sec, $\nu = 0.3$), and for two different deformation conditions. One sees that the difference between plane-strain and plane-stress assumptions is quite small. This is so because the boundary conditions are described in terms of tractions on the crack faces and the small difference is thus due to the slight change of elastic wave speeds under the two assumptions. Figure 14 provides the information about the stress level at any given distance from the crack tip and the moment of crack initiation for one particular test situation: choose a fixed distance δ, and the corresponding stress level in Figure 14 as σ_{cr}; using the dynamic initiation criterion, (4.1), the relationship between the apparent critical stress intensity factor K_{IC}^{d} and the time to fracture t_{cr} for any prescribed crack face pressure σ^*, can be determined. First, the critical time t_{cr} is calculated from (4.2) for the given crack face pressure σ^* and rise time T. Then the apparent dynamic fracture toughness K_{IC}^{d} is calculated from (4.3). The comparison between this analytical calculations and the experimental measurements is shown in Figures 15(a, b) for both plane-strain and plane-stress conditions. Once again, the difference between plane-strain and plane-stress is small. However, close examination reveals that the plane-strain condition is somewhat closer to the experimental results.

From Figures 15(a, b), one deduces that the model suggested in the previous section, captures the general trend of the experimental observations quite well. Ravi-Chandar and Knauss (1984) had suggested that fracture initiation is controlled by a time and rate invariant criterion for 'times' greater than about 50 to $60\,\mu\text{sec}$, while for shorter times or at higher rates of loading either the fracture criterion changes or the time dependent material behavior becomes important. However, the model proposed in this investigation, indicates that when the initiation time is larger than about $60\,\mu\text{sec}$, the loading rate does not have much effect on the fracture toughness. Conversely, it also showed that the marked increase in initiation toughness at high loading rates is the consequence of how fast (or slow) the stress reaches the critical level at the critical site. Therefore, the fracture initiation is really controlled by a unified mechanism.

References

Freund, L.B. (1972). Crack propagation in an elastic solid subjected to general loading–I. Constant rate extension. *Journal of the Mechanics and Physics of Solids* **20**, 129–140.

Freund, L.B. (1990). *Dynamic Fracture Mechanics*, Cambridge University Press.

Homma, H., Shockey, D.A. and Murayama, Y. (1983). Response of cracks in structural-materials to short pulse loads. *Journal of the Mechanics and Physics of Solids* **31**, 261–279.

Kalthoff, J.F. and Shockey, D.A. (1977). Instability of cracks under impulse loads. *Journal of Applied Physics* **48**, 986–993.

Krishnaswamy, S. and Rosakis, A.J. (1991). On the extent of dominance of asymptotic elastodynamic crack-tip fields: Part I – An experimetal study using bifocal caustics. *Journal of Applied Mechanics* **58**, 87–94.

Ma, C.C. and Freund, L.B. (1986). The extent of the stress intensity factor during crack growth under dynamic loading conditions. *Journal of Applied Mechanics* **53**, 303–310.

Petrov, Y.V. and Morozov, N.F. (1994). On the modeling of fracture of brittle solids. *Journal of Applied Mechanics* **61**, 710–712.

Ravi-Chandar, K. and Knauss, W.G. (1982). Dynamic crack-tip stresses under stress wave loading–a comparison of theory and experiment. *International Journal of Fracture* **20**, 209–222.

Ravi-Chandar, K. and Knauss, W.G. (1984). An experimental investigation into dynamic fracture: I. Crack initiation and arrest. *International Journal of Fracture* **25**, 247–262.

Ravi-Chandar, K. and Knauss, W.G. (1987). On the characterization of the transient stress field near the tip of a crack. *Journal of Applied Mechanics* **54**, 72–78.

Shockey, D.A., Kalthoff, J.F. and Erlich, D.C. (1983). Evaluation of dynamic crack instability criteria. *International Journal of Fracture* **22**, 217–229.

Shockey, D.A., Erlich, D.C., Kalthoff, J.F. and Homma, H. (1986). Short-pulse fracture mechanics. *Engineering Fracture Mechanics* **23**, 311–319.

Smith, G.C. (1975). An experimental investigation of the fracture of a brittle material. Ph.D. thesis, California Institute of Technology.

Steverding, B. and Lehnigk, S.H. (1970). Response of cracks to impact. *Journal of Applied Physics* **41**, 2096–2099.